2023 IEEE International Conference on Robotics and Automation (ICRA 2023)
May 29 - June 2, 2023. London, UK

A Soft Hybrid-Actuated Continuum Robot Based on Dual Origami Structures

Jian Tao, *Student Member, IEEE*, Qiqiang Hu, *Member, IEEE*, Tianzhi Luo, and Erbao Dong, *Member IEEE*

***Abstract*—Soft continuum robots have shown tremendous potential for medical and industrial applications owing to their flexibility and continuous deformability. However, their telescopic and bending capabilities and variable stiffness are still limited. This study proposes a novel origami-inspired soft continuum robot to possess large telescopic and bending capabilities while improving stiffness based on the principle of antagonistic actuation. The soft robot consists of dual origami structures. The inner forms an air chamber actuated by pneumatics, and the outer is controlled by nine tendon-driven actuators. The proposed design uses the advantages of a hybrid actuation to achieve motion and stiffness control. The performance of the soft robot is studied experimentally based on single and three robot modules. Results show that the robot has an excellent stretch ratio and a maximum bending angle of 180°. The robot can also increase stiffness to resist the bending deformation induced by self-weight and loads.**

Keywords: Soft robotics, continuum robots, origami robots, variable stiffness.

I. INTRODUCTION

Continuum robots usually have infinite motion degrees of freedom and can perform tasks in unstructured environments owing to their flexible structures. Therefore, they can handle interactive tasks with humans and show potential applications in invasive surgery, search and rescue, and structural inspection [1, 2]. However, continuum robots still have limitations in telescopic and bending capabilities and variable stiffness.

Different methods have been used to improve the stiffness of soft robots. Stiffness-tunable materials, such as low–melting point alloys [3, 4], electrorheological or magnetorheological fluids [5, 6], and shape memory polymers [7, 8, 9], have been utilized by controlling the temperature or magnetic field. These materials achieve variable stiffness by phase change, but recovering stiffness in a short time is usually challenging. Particle jamming was used to enhance stiffness and improve the grip robustness of soft hands owing to its low cost and fast response [10, 11]. By combining particle and layer jamming, soft robotic fingers can adapt to targeted objects at low stiffness and stably grasp the objects at high stiffness [12]. These jamming approaches improve stiffness by increasing friction and confrontation between particles or layered materials. However, such approaches usually decrease the telescopic or bending deformability of the robot. The self-locking joints improve the stiffness of the fingers through mechanical interlocking and achieve a large gripping force [13]. However, the mechanism-based approach is considerably complex regarding design and control. Antagonistic actuation can increase the internal stress of soft manipulators and realize bending, elongation, and hardening by applying forces in opposite directions [15, 16]. This method is easily applied in continuum robots and does not sacrifice the deformability of the robot.

Foldable origami structures provide a potential approach for developing continuum robots with large telescopic and bending deformations [17, 18]. Origami is usually super light but provides adjustable resilience through the crease design. It can maintain structural rigidity while enabling flexible deformation in compression and bending [19]. These unique properties of origami have been exploited in soft continuum robots [20, 21, 22]. For instance, an origami continuum robot provides high torsional stiffness for smooth motion control while maintaining high telescopic and bending deformability [20, 23]. A continuum robot is designed to greatly reduce its weight using origami patterns [22]. However, these origami continuum robots cannot change their stiffness to reduce gravity-induced deformation. A soft continuum robot presents the ability to enhance stiffness but loses large bending deformation and hardly achieves compression by combining pneumatics, particle jamming, and origami [24]. Therefore, soft continuum robots that can rapidly extend, compress, or bend variable stiffness are still to be studied.

The main contribution of this study is to design a novel soft continuum robot based on dual origami structures to achieve large telescopic and bending deformation and variable stiffness, which can perform tasks in some special narrow and complex spaces. The robot comprises three modules, each of which uses dual origami as the skeleton. The inner origami forms an air chamber actuated by pneumatics, and the outer origami is controlled by nine tendon-driven actuators. The robot can quickly extend or retract in the axial direction through the pneumatic actuation and bend along multiple directions by the tendon-driven actuation. The stiffness improvement is achieved based on

The authors thank for the support of the National Natural Science Foundation of China under Grant No. 61773358 and the support of the Students' Innovation and Entrepreneurship Foundation of USTC No. CY2022G36. (*Corresponding authors: Erbao Dong and Tianzhi Luo*)

Jian Tao, Erbao Dong, and Tianzhi Luo are with the CAS Key Laboratory of Mechanical Behavior and Design of Materials, the School of Engineering Science, University of Science and Technology of China, Hefei 230026, China (e-mail: jiantao@mail.ustc.edu.cn; ebdong@ustc.edu.cn; tzluo@ustc.edu.cn).

Qiqiang Hu is with the Department of Biomedical Engineering, City University of Hong Kong, Kowloon, Hong Kong (e-mail: qiqianghu3-c@my.cityu.edu.hk).

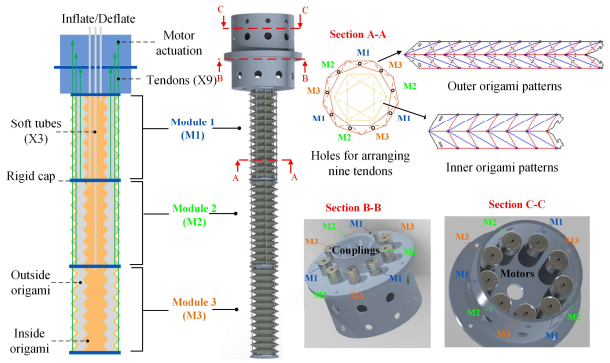

Fig. 1. The structure design of the soft continuum robot. The robot is divided into three modules, which are composed of inner and outer origami, tendons, soft tubes, and a rigid cap. Nine tendons are distributed around the outer origami in Section A-A, corresponding to nine couplings actuated by motors in Section B-B.

the antagonistic effect of the hybrid actuation of pneumatic and tendon-driven actuators. The proposed soft continuum robot can be serially assembled with multiple modules to reach the required length in practical applications, thereby obtaining enough working space. Each robot module can achieve independent telescopic and bending deformation through hybrid actuation.

The remainder of this paper is organized as follows: Section II describes the modular robot design and fabrication. Section III presents the experimental studies on a single robot module, including stiffness, load, and bending tests. Section IV presents some experiments on the soft continuum robot to show the advantages of the hybrid actuation of pneumatic and tendon-driven actuators. The grasping experiments are also conducted by combining a soft gripper to demonstrate the potential applications of the robot. Section V concludes the study and provides a discussion of future works.

II. Design and Fabrication

A. Robot Design

Fig. 1 shows the design of the proposed soft continuum robot, which is mainly composed of an inner origami structure sealed up and an outer origami structure that arranges nine tendons. The dual origami structures serve as the robot skeleton. This design combines the advantages of pneumatic (internal) and tendon-driven (external) actuation. The shape parameters [n, L, W] can be directly used to define the cross-sectional shape of the origami according to our previous design model [25], where n is the number of sides, L is the length of the sides, and W is the thickness of the sides. According to the functional requirements of the robot, the cross-sectional shapes of the inner and outer origami are designed to be [6, 20 mm, 10 mm] and [9, 20 mm, 7 mm], respectively. The flat crease patterns of the origami and the shape parameters can be obtained from the inverse design software that we developed [26].

The stiffness of the soft continuum robot can be adjusted by controlling the air pressure of the inner origami and the tension of tendons. Nine tendons (diameter: 0.33 mm, PE line) are evenly distributed around the outer origami structure at 40° intervals. Each module has an independent

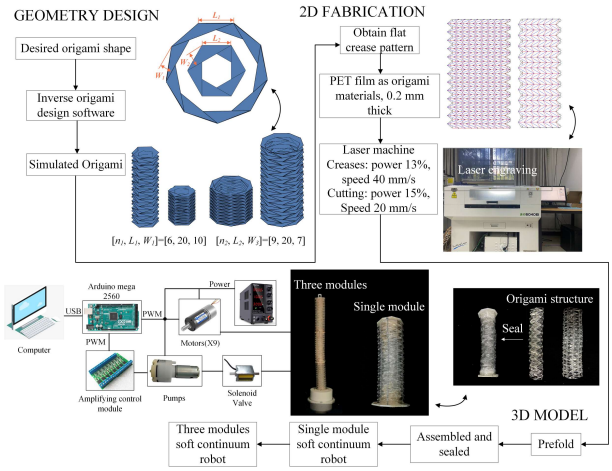

Fig. 2. Manufacturing process of the soft continuum robot, including geometry design, 2D fabrication, and 3D model.

air chamber. The holes remaining in the outer origami can guide the path of the tendons. According to the cross-sectional views of A-A and B-B in Fig. 1, the tendons are connected to nine couplings actuated by brushless motors (GA24Y-2418, gear ratio 320:1). The motor provides a maximum torque of 6 kg·cm, and its output force can reach 61.9 N. When the tendon is pulled, the soft continuum robot can bend in one direction. The inner origami structure is sealed with thin, sticky tape, and both ends are covered with two caps while a soft air tube is inserted to provide power. The soft tube is connected to a motor pump, which is controlled by a magnetic valve to deflate and inflate the inner origami. When the inner origami is deflated, the soft continuum robot can contract quickly. An Arduino Mega 2560 board is used to receive commands from the computer and control the actions of motors and air pumps. The motor can pull the tendons to change the attitude of the soft continuum robot. Combined with tendon-driven actuation, the inner origami can be inflated to improve the stiffness of the robot based on antagonistic actuation. Meanwhile, each robot module can achieve independent telescopic and bending motions owing to the controlled stiffness.

B. Manufacturing Process

Fig. 2 shows the manufacturing process of the soft continuum robot, which can be divided into three steps as follows.

Step I: The origami shapes are first simulated in the inverse origami design software [26] to obtain the suitable shape parameters [n, L, W] of the outer and inner origami structures. The flat crease patterns of the origami are then generated. The hole patterns for arranging the tendons and locking patterns are also added.

Step II: A laser cutting machine (Suqie 6040B, Han's Yueming Laser Group Co., Ltd., China) is used to write the generated crease patterns on the back and front of a polyethylene terephthalate (PET) film (thickness: 0.2 mm). The laser power and speed used for engraving the creases are 13% and 40 mm/s, and the power and speed used for cutting the edges are 15% and 20 mm/s, respectively. Origami with different folding stiffness can be made by adjusting the engraving power or speed.

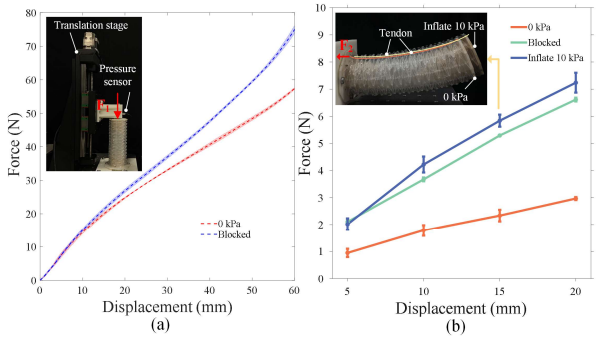

Fig. 3. Test compressive and bending stiffness. (a) The results of the compressive stiffness under the environment of 0 kPa and blocked soft tube orifice. (b) The results of the bending stiffness under different environments.

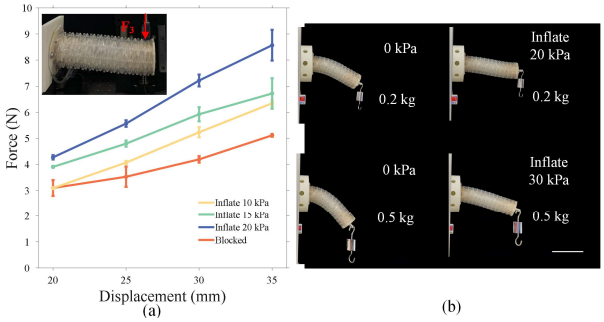

Fig. 4. Test lateral stiffness. (a) The results of the lateral stiffness under different inflation pressures. (b) The actual performance of the module under different lateral loads of 0.2 and 0.5 kg. The scalar bar is 100 mm.

Step III: Finally, 3D origami structures of expected folded shapes and sizes are obtained by prefolding. The rigid caps at both ends of each module are printed using a 3D printer. The inner origami is sealed with thin, sticky tape and rigid caps and then assembled with the outer origami. Nine tendons pass through the holes on each side of the outer origami and attach to the couplings. These couplings are distributed annularly and fixed on the rotating shafts of the motors. The assembled soft continuum robot has an original length of 519 mm, a maximum diameter of 58.48 mm, and a weight of 242.22 g, not including motors. When fully extended, its length is 591 mm. The minimum length of 269 mm can be achieved by shrinking. The robot can integrate pneumatic and tendon-driven actuators to achieve large deformation and variable stiffness.

III. Experimental Studies on the Single Robot Module

The single module of the soft continuum robot is first investigated in this section, including the stiffness test, load capacity, and bending capacity.

A. Stiffness Test

The stiffness test is performed on a high-precision motion platform at a speed of 1.0 mm/s, and the resulting force is measured using a force sensor (JLBS-M2). Each test was repeated three times. In this study, we defined the initial pressure of the chamber as 0 kPa. The stiffness value can be estimated as follows:

$$K = F/x\,, \tag{1}$$

where F is the recorded value by the force sensor, and x is the generated displacement under F. Then, the influences of different environments on the stiffness of the module are studied. The compression stiffness at 0 kPa was tested first, as shown in Fig. 3(a). As a comparison, the air tube was also blocked to evaluate the stiffness, where the chamber pressure will increase with the compression of the module. When the module was compressed by 60 mm, the measured forces (F_1) can reach 57.4 and 75.0 N under 0 kPa and blocked state, respectively. The compressive stiffness of the blocked module can be estimated as 1.25 N/mm. The blocked chamber generates a high pressure under the same compression, thereby resulting in high resistance force and compressive stiffness.

When a tendon was connected to a force sensor and pulled to bend the module, the tension force of the tendon (F_2) was measured by the force sensor to evaluate the bending stiffness of the module. Fig. 3(b) shows the tested results when the inner origami was under 0 kPa and blocked and inflated states. When the tendon was pulled by 20 mm, F_2 reached a value of 2.97 N at 0 kPa. Given that the blocked state increases the air pressure of the internal chamber, F_2 reached 6.62 N. When the inner origami was inflated at 10 kPa, F_2 reached 7.24 N because of the high chamber pressure. The bending stiffness of the inflated module can be estimated as 0.36 N/mm which is increased four times by pressurization. Therefore, inflation can increase F_2, thereby improving the bending stiffness. In addition, Fig. 3(b) shows that a large amount of compression always accompanies the bending of the module at 0 kPa. However, the inflation can considerably counteract the generated compression, allowing the module to bend without compression. The results also show that the inflated module has a large bending amplitude under the same F_2, which can improve the practical performance of the soft continuum robot.

When different lateral displacements are applied to the tip of the module, the generated forces (F_3) are recorded by the force sensor to evaluate the lateral stiffness of the module. Fig. 4(a) shows the tested results. The force F_3 increases almost linearly with the lateral displacement and increases as the inflation pressure rises. When the applied lateral displacement was 35 mm, the average F_3 reached 5.12, 6.35, 6.72, and 8.57 N under inflation of 0, 10, 15, and 20 kPa, respectively. That indicates that the lateral stiffness of the module can be adjusted by controlling the inflation pressure. The lateral stiffness of the module in the Fig. 4(a) is estimated as 0.24 N/mm which is almost three times as the robot [15]. High stiffness can prevent the lateral deformation of the module and increase the load capacity. The effect of inflation on the lateral stiffness of the module is further presented based on two groups of comparative experiments, as shown in Fig. 4(b). When not inflated, the module has a large lateral deformation under loads of 0.2 and 0.5 kg at the tip. After being inflated at 20 and 30 kPa, the module has a markedly reduced lateral deformation. Therefore, inflation can enhance the resistance to external loads and improve the performance of the robot.

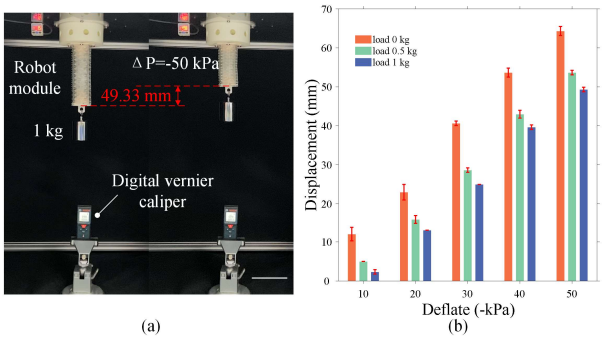

Fig. 5. Test telescopic capacity. (a) The physical image of the module lifting a load of 1 kg and moving 49.33 mm. (b) The telescopic capacity under different loads and deflation pressures. The scalar bar is 100 mm.

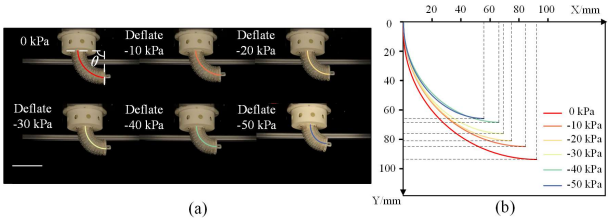

Fig. 6. Test bending capacity. (a) The physical image and (b) the results of the end position of the module with a bending angle of 90° under different deflation pressures. The scalar bar is 100 mm.

B. *Telescopic and Bending Capabilities*

The telescopic capability of the module is evaluated by the expansion ratio. The minimum (L_{min}) and maximum (L_{max}) lengths of the module are measured when fully retracted and extended. The expansion rate δ_L is defined as follows:

$$\delta_L = \frac{L_{max} - L_{min}}{L_{min}}. \tag{2}$$

The L_{min} and L_{max} of the module are 87 and 197 mm, respectively. Therefore, δ_L of the module is 126.4%. The telescopic capability of the module is tested in detail under different loads, as shown in Fig. 5. The loads are hung at the end of the module. The output displacement generated by the module is measured using a digital vernier caliper. The results show that the module can generate maximum output displacements of 64.33, 53.67, and 49.33 mm under different loads of 0, 0.5, and 1 kg, respectively, and the same deflation pressure of −50 kPa. The output displacement increases with the increasing deflation pressure, and the load capacity of the module can be further improved by increasing the deflation pressure. The deflation can balance the gravitational effect of the load and maintain the load at a certain height.

Fig. 6 shows the bending behaviors of the module. In the experiments, the same tendon of the module was actuated, and different deflation pressures were used. The angle between the planes on which the rigid caps at both ends lie is defined as the bending angle θ. The tendon was pulled to make θ reach 90° at each test. Fig. 6(a) shows the bending attitudes of the module under the actuation of different deflation pressures. The module shrinks more evidently as the deflation pressure increases, thereby making the end of the module arrive at different positions.

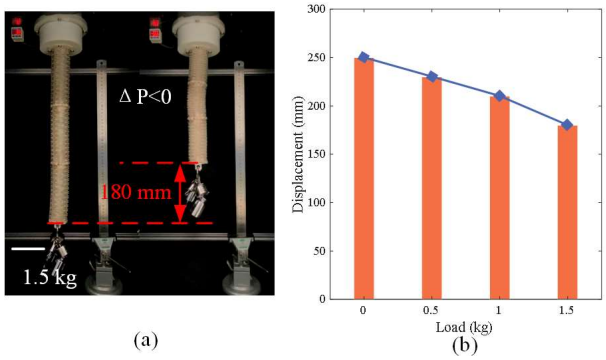

Fig. 7. Test telescopic deformation of the robot. (a) The physical image of the robot lifting a load of 1.5 kg and moving 180 mm. (b) The output displacement under different loads. The scalar bar is 100 mm.

The neutral lines of these modules are extracted and drawn in Fig. 6(b) to show their difference visually. Using different deflation pressures can improve the working space of the module. Therefore, the robot will be able to perform specific operational tasks in a large working space.

IV. Demonstration of the Soft Continuum Robot

After investigating the characterizations of the single module, a soft continuum robot based on the three same modules is assembled and tested. The robot will show a large telescopic and bending deformation and variable stiffness. The robot can demonstrate the ability to grasp different objects continuously by incorporating a Fin Ray gripper.

A. *Large Telescopic Deformation*

The soft continuum robot was fixed on a test bench assembled by aluminum profiles. The L_{min} and L_{max} of the robot are 269 and 591 mm, respectively. Therefore, the δ_L of the robot is 119.7%. We hung different loads of 0.5, 1, and 1.5 kg at the end of the robot and then applied the deflation to each robot module. The robot shrinks and lifts the loads. The output displacement was tested, as shown in Fig. 7. The results show that the robot can generate a displacement of 250 mm when there is no load in the natural state. When hanging loads of 0.5, 1.0, and 1.5 kg, the robot generated displacements of 230, 210, and 180 mm, respectively. The output displacement decreases with the increasing load. These tests only used pneumatic actuation to show the telescopic capability of the robot, which may be improved by combining tendon-driven actuation simultaneously.

B. *Variable Stiffness*

We placed the robot horizontally to show the variable stiffness capacity of the soft continuum robot, as shown in Fig. 8(a). When the robot did not use any actuators, the robot sagged naturally because of the gravitational effect. However, the robot can considerably resist the deformation induced by gravity after inflating the inner origami. Furthermore, we hung a load of 0.5 kg at the end of the robot. Modules 2 and 3 of the robot were inflated by 10 kPa, module 1 was deflated to full retraction, and all the tendons were pulled to tighten the robot. Then, the robot will be in a high stiffness state and can hang the load with little deformation, as shown in Fig. 8(b). The robot hardly

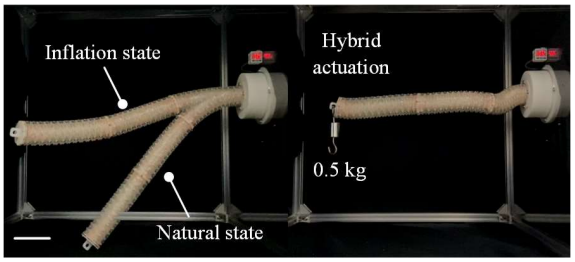

Fig. 8. Test variable stiffness of the robot. (a) Comparison of the natural state and inflation state. (b) Stiffness test under a 0.5 kg load. The scalar bar is 100 mm.

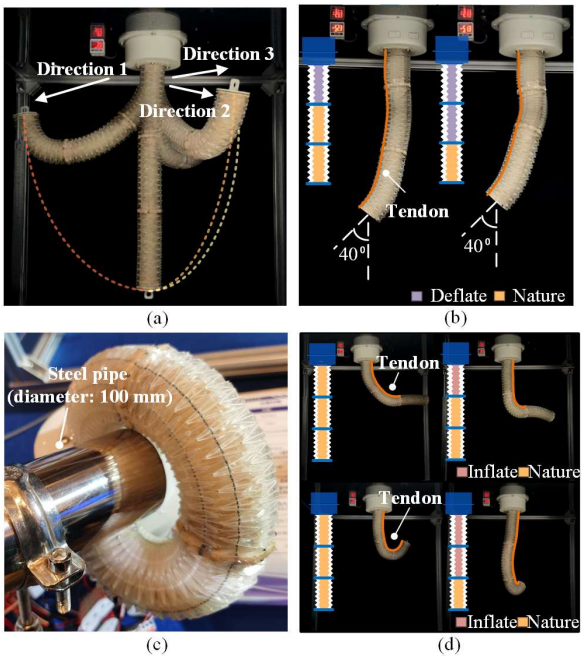

Fig. 9. Test the bending deformation of the robot. (a) Motion range of the robot. (b) The robot positions under different deflated modules when the yaw angles are 40°. (c) The winding test of the robot. (d) Independent bending motion of modules 2 and 3.

performs the telescopic motion under the antagonistic effect, which requires precise control of the chamber pressure and tension of the tendons. The experimental results verify the effectiveness of the hybrid actuation of pneumatic and tendon-driven actuation in adjusting the robot stiffness.

C. Large Bending Deformation

Fig. 9(a) shows the large bending deformation of the soft continuum robot. The three longest tendons attached to module 3 were pulled to bend the robot by 180° in three directions from the natural vertical state. A large working space of the robot can be achieved by combining the tendon-driven actuation and different deflation pressures, as shown in Fig. 9(b). In the experiments, the same tendon of the module was actuated, and different modules were deflated. The yaw angle between the normal direction of the end cap and the vertical direction reached 40° in each test. However, the end cap of the robot arrived at different positions when module 1 was deflated solely and modules 1 and 2 were deflated simultaneously. This case proves that the working space of the robot can be conveniently

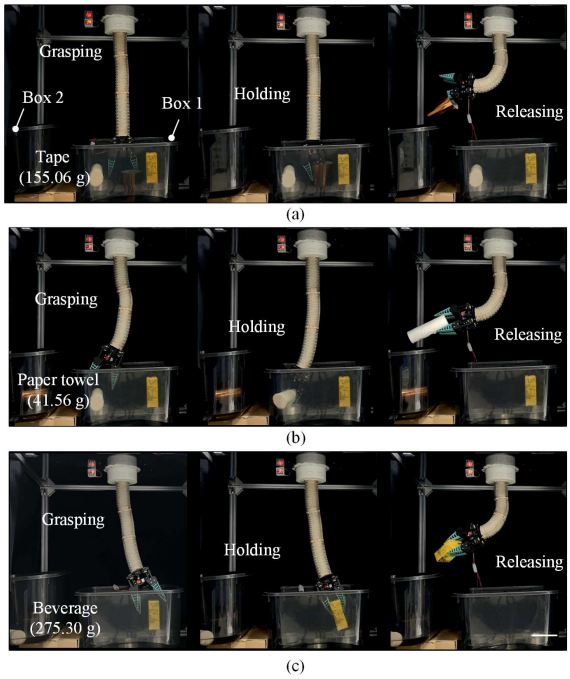

Fig. 10. The robot continuously grasps (a) tape (155.06 g), (b) paper towel (41.56 g), and (c) beverage (275.30 g). The scalar bar is 100 mm.

improved by combining tendon-driven and pneumatic actuation. Fig. 9(c) shows the winding capacity of the soft continuum robot. The robot can wrap around a steel pipe (diameter: 100 mm) horizontally placed for a circle, showing its strong bending capability and flexibility.

Traditional rear-mounted continuum robots usually keep the front-end robot light and compact, but achieving the independent actuation of each joint is difficult. The independent motion of each joint can greatly improve the working space and adaptability of the robot. The variable stiffness can be used to address this problem in this study. Fig. 9(d) shows two groups of comparison experiments to illustrate how to control the independent motion of modules 2 and 3. Module 1 can easily achieve an independent motion by solely actuating the tendons attached to this module. When the tendon attached to module 2 was actuated, the robot usually bent modules 1 and 2. However, when module 1 was inflated at 20 kPa for high stiffness, the actuation of tendons only bent module 2, and module 1 approximately remained vertical. Similarly, when the tendon attached to module 3 was pulled, the robot bent all the modules. The independent bending of module 3 can be achieved by inflating modules 1 and 2 at 20 kPa. The results show that the variable stiffness can greatly expand the bending capability of the continuum robot.

D. Grasping Experiments

A Fin Bay gripper was fixed at the end of the soft continuum robot to assist in grasping the objects, which was controlled by a servo motor, as shown in Fig. 10. The robot continuously grasped different objects, such as tape, paper towel, and beverage, from box 1 and then placed them into box 2. After releasing the tape into box 2, the motors were reversely rotated to relax the tendons, allowing the robot back to a vertical state. Then, modules 1 and 2

were inflated to increase the length of the robot while adjusting the attitude of the gripper to grasp the paper towel in box 1. Then, modules 1 and 2 were fully deflated, and the motors were rotated to pull tendons to bend the robot. After reaching the release point, the gripper opened to release the paper towel into box 2. The weights of these objects showed no effect on the motion capability of the robot. Moreover, the robot can easily manipulate them using hybrid pneumatic and tendon-driven actuation. The results demonstrate the potential application of the robot in manipulating objects.

V. Conclusion and Future Work

This study proposed a soft continuum robot based on dual origami structures and hybrid actuation, thereby achieving large telescopic and bending deformation and variable stiffness. The robot can bend in multiple directions by actuating different tendons and quickly reduce by deflating. The robot can increase the stiffness based on the principle of antagonistic actuation. Meanwhile, each robot module can be independently actuated owing to the variable stiffness. The expansion ratios of the single module and the robot reach δ_L = 126.4% and δ_L = 119.7%, respectively. Combined with these features, the robot can achieve large telescopic and bending deformation using multiple modules. That is, the curvature of each module can be solely changed by hybrid actuation. The resulting robot can work in narrow and complex spaces, showing promising applications.

The experimental studies were conducted in detail to investigate the compressive, bending, and lateral stiffness of the single robot module. The compressive stiffness increases almost linearly with the compression. In addition, the bending stiffness rises linearly with the increasing inflation pressure. Experiments also demonstrate that hybrid pneumatic and tendon-driven actuation can improve the lateral stiffness and load capacity. Finally, the potential application of the soft continuum robot in the gripper is presented by the grasping experiments.

Future works can incorporate the visual perception system into the soft continuum robot to assist the robot in precisely detecting and grasping objects. The design and optimization of the motion trajectory of the soft continuum robot will be further studied.

References

[1] D. Rus and M. Tolley, "Design, fabrication and control of soft robots," *Nature*, vol. 521, no. 7553, pp. 467-475, 2015.

[2] H. Jiang et al., "Hierarchical control of soft manipulators towards unstructured interactions," *The International Journal of Robotics Research*, vol. 40, no. 1, pp. 411-434, 2021.

[3] Y. F. Hao et al., "A eutectic-alloy-infused soft actuator with sensing, tunable degrees of freedom, and stiffness properties," *Journal of Micromechanics and Microengineering*, vol. 28, no. 2, Art. no. 024004, 2018.

[4] B. E. Schubert and D. Floreano, "Variable stiffness material based on rigid low-melting-point-alloy microstructures embedded in soft poly(dimethylsiloxane) (PDMS)," *Rsc Advances*, vol. 3, no. 46, pp. 24671-24679, 2013.

[5] G. Park, M. T. Bement, D. A. Hartman, R. E. Smith, and C. R. Farrar, "The use of active materials for machining processes: A review," *International Journal of Machine Tools & Manufacture*, vol. 47, no. 15, pp. 2189-2206, 2007.

[6] S. B. Behbahani and X. B. Tan, "Design and dynamic modeling of electrorheological fluid-based variable-stiffness fin for robotic fish," *Smart Materials and Structures*, vol. 26, no. 8, Art. no. 085014, 2017.

[7] Y. J. Chen, J. Sun, Y. J. Liu, and J. S. Leng, "Variable stiffness property study on shape memory polymer composite tube," *Smart Materials and Structures*, vol. 21, no. 9, Art. no. 094021, 2012.

[8] W. Wang and S.-H. Ahn, "Shape memory alloy-based soft gripper with variable stiffness for compliant and effective grasping," *Soft Robotics*, vol. 4, no. 4, pp. 379-389, 2017.

[9] Y. Yang, Y. Chen, Y. Li, Z. Wang, and Y. Li, "Novel variable-stiffness robotic fingers with built-in position feedback," *Soft Robotics*, vol. 4, no. 4, pp. 338-352, 2017.

[10] J. Zhou et al., "Adaptive Variable Stiffness Particle Phalange for Robust and Durable Robotic Grasping," *Soft Robotics*, vol. 7, no. 6, pp. 743-757, 2020.

[11] Y. Wei et al., "A Novel, Variable Stiffness Robotic Gripper Based on Integrated Soft Actuating and Particle Jamming," *Soft Robotics*, vol. 3, no. 3, pp. 134-143, 2016.

[12] Y. Yang, Y. Zhang, Z. Kan, J. Zeng, and M. Y. Wang, "Hybrid Jamming for Bioinspired Soft Robotic Fingers," *Soft Robotics*, vol. 7, no. 3, pp. 292-308, 2020.

[13] Q. Hu, H. Huang, E. Dong, and D. Sun, "A Bioinspired Composite Finger With Self-Locking Joints," *IEEE Robotics and Automation Letters*, vol. 6, no. 2, pp. 1391-1398, 2021.

[14] Y. Yang, Y. T. Li, and Y. H. Chen, "Principles and methods for stiffness modulation in soft robot design and development," *Bio-Design and Manufacturing*, vol. 1, no. 1, pp. 14-25, 2018.

[15] A. Stilli, H. A. Wurdemann, K. Althoefer, "Shrinkable, stiffness-controllable soft manipulator based on a bio-inspired antagonistic actuation principle," *IEEE/RSJ International Conference on Intelligent Robots and Systems (IROS)*, Chicago, IL, pp. 2476-2481, 2014.

[16] K. Althoefer, "Antagonistic actuation and stiffness control in soft inflatable robots," *Nature Reviews Materials*, vol. 3, no. 6, pp. 76-77, 2018.

[17] W. Kim, J. Eom, and K.-J. Cho, "A Dual‐Origami Design that Enables the Quasisequential Deployment and Bending Motion of Soft Robots and Grippers," *Advanced Intelligent Systems*, vol. 4, no. 3, Art. no. 2100176, 2021.

[18] K. Zhang, C. Qiu, and J. S. Dai, "An Extensible Continuum Robot With Integrated Origami Parallel Modules," *Journal of Mechanisms and Robotics*, vol. 8, no. 3, Art. no. 031010, 2016.

[19] E. V. Hoff, J. Donghwa, and L. Kiju, "OrigamiBot-I: A thread-actuated origami robot for manipulation and locomotion," *IEEE/RSJ International Conference on Intelligent Robots and Systems (IROS)*, Chicago, IL, pp. 1421-1426, 2014.

[20] J. Santoso and C. D. Onal, "An Origami Continuum Robot Capable of Precise Motion Through Torsionally Stiff Body and Smooth Inverse Kinematics," *Soft Robotics*, vol. 8, no. 4, pp. 371-386, 2021.

[21] D. Jeong and K. Lee, "Design and analysis of an origami-based three-finger manipulator," *Robotica*, vol. 36, no. 2, pp. 261-274, 2017.

[22] Y. Xu, Q. Peyron, J. Kim, and J. Burgner-Kahrs, "Design of Lightweight and Extensible Tendon-Driven Continuum Robots using Origami Patterns," *IEEE International Conference on Soft Robotics (RoboSoft)*, New Haven, CT, USA, pp. 308-314, 2021.

[23] J. Santoso, E. H. Skorina, M. Luo, R. Yan, and C. D, "Design and Analysis of an Origami Continuum Manipulation Module with Torsional Strength," *IEEE/RSJ International Conference on Intelligent Robots and Systems (IROS)*, Vancouver, CANADA, pp. 2098-2104, 2017.

[24] Y. Li, T. Ren, Y. Chen, and M. Z. Q. Chen, "A Variable Stiffness Soft Continuum Robot Based on Pre-charged Air, Particle Jamming, and Origami," *IEEE International Conference on Robotics and Automation (ICRA)*, ELECTR NETWORK, pp. 5869-5875, 2020.

[25] Q. Hu, "Research on Soft Robot Design for Grasping and Climbing Scenarios," Ph.D. dissertation, City University of Hong Kong, Hong Kong, 2022.

[26] Q. Hu, "Inverse-Origami-Design-Model," [Source code], 2022. [Online]. Available: https://github.com/Flourishingsky/Inverse-Origami-Design-Model.git